Applied Catalysis B: Environmental 147 (2014) 236–245

Contents lists available at ScienceDirect

Applied Catalysis B: Environmental

journal homepage: www.elsevier.com/locate/apcatb

Hydrogenolysis of methyl heptanoate over Co based catalysts: Mediation of support property on activity and product distribution

Qiying Liu [a], Yuwei Bie [b], Songbai Qiu [a], Qi Zhang [a], Jani Sainio [c], Tiejun Wang [a,*], Longlong Ma [a,**], Juha Lehtonen [b]

[a] CAS Key Laboratory of Renewable Energy, Guangzhou Institute of Energy Conversion, Chinese Academy of Sciences, Guangzhou 510640, PR China
[b] Department of Biotechnology and Chemical Technology, Aalto University, P.O. Box 16100, 00076 Aalto, Finland
[c] Department of Applied Physics, Aalto University, P.O. Box 16100, 00076 Aalto, Finland

ARTICLE INFO

Article history:
Received 14 June 2013
Received in revised form 31 July 2013
Accepted 28 August 2013
Available online 5 September 2013

Keywords:
Methyl heptanoate
Hydrogenolysis
Co catalyst
Support property
Product distribution

ABSTRACT

Co/MgO, Co/SiO_2 and Co/Hβ catalysts were prepared by incipient wetness impregnation. The formation of MgO-CoO solid solution and $MgCo_2O_4$ spinel in Co/MgO resulted in high dispersions of Co on MgO even at the low calcined temperatures and the high Co loadings. The second impregnation of Co on Co/MgO enhanced Co cations in surface/subsurface of catalysts, which led to the enlarged metallic Co particle sizes by H_2 reduction. Comparatively, the highly dispersion of Co was only observed on SiO_2 and Hβ at the low Co loadings owing to the $Co^{\delta+}$ species of strong interactions with these supports. The solid solution/spinel and the strongly interacted $Co^{\delta+}$ species induced the Co cations reduced at higher temperatures with obtaining the small Co particle sizes. These cases also significantly decreased the basicities of Co/MgO depending on calcined temperature and Co loadings, and increased the acidic sites of Co/SiO_2 and Co/Hβ with obtaining enhanced acidities, respectively. During hydrogenolysis processing, the basic sites of Co/MgO triggers the splitting of acyl C—O bond of methyl heptanoate to form heptanal and methanol, followed by further hydrogenation of heptanal to 1-heptanol. While the acidic Co/SiO_2 and Co/Hβ induce the cracking of ether C—O bond to heptanoic acid and CH_4. Heptanoic acid intermediate is then converted into C_6 and C_7 alkanes by the parallel decarbonylation and HDO pathways, respectively. The activity and product distribution could be facilely mediated by the synergistic catalysis of metal and acid/base. Under optimal conditions, the maximal 1-heptanol and summed C_6/C_7 alkanes yields of 55% and 89% were observed over Co/MgO and Co/SiO_2 with desire Co loadings, respectively, indicating the promising applications of these catalysts in hydrogenolysis of vegetable oils.

1. Introduction

As a unique and renewable carbon resource, vegetable oils could be effectively converted into diversified chemicals used in fine chemical industries as surfactants and plasticizers [1] and hydrocarbon fuels for sustaining our society development as fossil energy replacement [2,3]. Production of these biomass derived chemicals and fuels is considered to significantly diminish negative impacts on environment, due to that biomass hardly contains sulfur and presents the property of CO_2-neutral (CO_2 released during biomass utilization can be used for biomass growth in the next cycle) [4].

Aliphatic alcohols with long carbon chains could be produced by hydrogenolysis of fatty esters obtained via transesterification of vegetable oils [5]. Cu–Cr catalyst was proven to be effective for this processing under severe reaction conditions of high temperatures and H_2 pressures [6]. However, the use of toxic Cr is currently discouraged and the severe reaction conditions are undesirable. Thus, exploring the catalysts without Cr to produce higher alcohols above mentioned under mild reaction conditions is of practical importance. The present catalysts used mainly focus on the supported noble metals Ru [7–9], Rh [8] and Pt [10], and the transition metals Cu [11–13], Ni [14] and Co [15–17]. The pristine metals usually show low activities as well as selectivities due to parallel side reactions. As B, Sn, Mo, Mn, Fe oxide additives are introduced, the performance can be significantly improved owing to the partially oxidic additives promote activation of fatty ester as Lewis acid and accelerates its conversion to higher alcohols [18].

On the other hand, renewable hydrocarbon fuels could be also produced by catalytic hydrodeoxygenation (HDO) of vegetable oils and/or fatty esters as model compounds [19,20]. These hydrocarbon fuels hardly contain oxygen and unsaturated C—C bonds, which shows superior fuel properties of high chemical stability,

* Corresponding author. Tel.: +86 20 87057751; fax: +86 20 87057737.
** Corresponding author. Tel.: +86 20 87057673; fax: +86 20 87057673.
E-mail addresses: wangtj@ms.giec.ac.cn (T. Wang), mall@ms.giec.ac.cn (L. Ma).

0926-3373/$ – see front matter © 2013 Elsevier B.V. All rights reserved.
http://dx.doi.org/10.1016/j.apcatb.2013.08.045

high caloric value and complete compatibility with gas engine to biodiesels produced by transesterification of vegetable oils with methanol [21]. Catalysts for this processing mainly contain supported sulfided Mo and W modified by Co and Ni [22–24], noble metal Pt and Pd [25,26], transition metal Ni [27,28] and metal phosphide and carbide Ni_2P [29], Mo_xC [30] and NiMoP [31]. The sulfided catalysts showed high activity and stability in HDO of vegetable oils, but the sulfur contained agents are necessary during pretreatment of catalysts and HDO processing, which inevitably brings about sulfur contamination in final products. Metal phosphide and carbide presented high selectivity for diesel ranged hydrocarbons, however, the preparation procedures of catalysts are tedious and rigorous, and transformation of active phases were usually observed during HDO of vegetable oils, leading to the limited lifetimes of such kind catalysts.

For hydrogenolysis and HDO of vegetable oils to higher alcohols and hydrocarbon fuels, acid–base properties of support played the essential role in mediating activity and product selectivity [27,32]. For example, catalysts with strong acidities showed severe cracking C_1–C_4 alkanes [27], while those with basicities have the high selectivity to heavy alkanes with carbon number of more than 35 due to significant ketonization coupling of fatty acid intermediates [32]. Co catalysts show promising performance in diversified hydrogenation/hydrogenolysis reactions. Using supported Co catalysts with mediated acid–base properties for selective conversion of vegetable oils into chemicals and hydrocarbon fuels is of scientific importance, but this is seldom reported in literature.

In this work, we prepared Co supported on basic MgO, neutral SiO_2 and acidic Hβ catalysts by incipient wetness impregnation and characterized their physical chemical properties by XRD, BET, H_2-TPR, CO_2/NH_3-TPD, H_2-chemosorption and TPSR techniques. The performance of supported Co catalysts were compared in hydrogenolysis of methyl heptanoate (the model compound of vegetable oils) to 1-hetpanol and hydrocarbon fuels and the hydrogenolysis pathways were discussed based on the acid–base properties of catalysts.

2. Experimental

2.1. Catalyst preparation

MgO was obtained from Aldrich Chemicals Co. Ltd., SiO_2 was gained from Aladdin Chemicals Co. Ltd. for SiO_2 and Hβ (Si/Al = 25) was got by Tianjin Nankai Catalyst Company. The analytical graded chemicals including $Co(NO_3)_2{\cdot}6H_2O$, methyl heptanoate, n-hexadecane, cumene, heptanoic acid, heptanal, 1-heptanol, heptyl heptanoate, methanol, heptane, hexane and methyl acetate were purchased from Aldrich Chemicals Co. Ltd. and used without further purification.

The supported Co catalysts were prepared by incipient wetness impregnation. $Co(NO_3)_2{\cdot}6H_2O$ was dissolved in aqueous solution with the concentration of 0.1 M and a certain amount of support was added to gain a desire Co loading by weight. The resultant suspension was stirred for 10 h at ambient temperature, followed by evaporating excessive water at 353 K. The solid remained was dried at 393 K and calcined at a certain temperature for 4 h in air (for Co/SiO_2 and Co/Hβ, the calcined temperature was fixed at 823 K). For Co supported on MgO, a second Co impregnation was implemented by the similar procedure mentioned above. The 10%Co/MgO was calcined at 1273 K and then used as support for the sequential impregnation with different Co loadings, followed by drying at 393 K and calcining at 823 K for 4 h. All the samples were reduced at 823 K for 2 h under H_2 flow before reaction.

2.2. Catalyst characterization

XRD patterns of catalysts were obtained with using X'pert PRO MPD diffract meter (PANalytical) operated at 40 kV and 40 mA with a Cu Kα (λ = 0.15406 nm) radiation. BET surface, external surface and mesoporosity of catalysts were determined by the adsorption-desorption behavior of N_2 at 77 K using a Micrometrics ASAP-2010 automated system. H_2-TPR, CO_2-TPD and NH_3-TPD experiments were carried out in a home-made instrument equipped with a thermal conductivity detector (TCD). For H_2-TPR analysis, the samples were pretreated at 673 K for 0.5 h under N_2 flow. The samples were cooled down to room temperature and then programmed to 1273 K at a ramp of 10 K/min under 5%H_2/N_2. For CO_2-TPD measurements of Co/MgO, the samples were pretreated at 823 K for 2 h, cooled down to 323 K in He and absorbed by CO_2. The CO_2 absorbed catalysts were purged by He at the same temperature to remove the physically absorbed CO_2. The samples were then heated from 323 K to 823 K at the rate of 10 K/min in He. The NH_3-TPD measurements of Co/SiO_2 and Co/Hβ were similar to the CO_2-TPD procedure while with the absorbing and purging temperature maintained at 393 K and the final temperature was set at 900 K. H_2-chemisorption measurements were tested with using a Quantachrome-ASIQACIV200-2 automated gas sorption analyzer. The catalysts were reduced at 823 K for 2 h under flow H_2. After reduction, the samples were further heated to 873 K in He to clean the catalyst surface, and then were cooled down to 323 K for H_2-chemisorption tests. The TPSR measurements of methyl acetate were carried out on a ChemBet Pulsar instrument (Quantachrome, USA) equipped with a mass spectrometer (Ametek DYCOR LC-D200, USA). The samples were reduced at 823 K for 2 h under H_2 and were cooled down to ambient temperature for absorbing methyl acetate until saturation and then were purged by He for 0.5 h. The samples were heated to 750 K at 12 K/min under a H_2 flow of 40 ml/min.

2.3. Hydrogenolysis of methyl heptanoate

Hydrogenolysis of methyl heptanoate was conduced in a 100 ml stainless steel autoclave with a Teflon inner and a mechanical stirring. Typically, a mixture of 0.5 g methyl heptanoate dissolved in 20 g n-hexadecane was loaded into the autoclave, followed by adding 0.15 g of freshly reduced catalyst. Before reaction, the system was flushed by N_2 to remove air residue and was pressurized to 3 MPa of H_2, which was then heated to 493 K and kept at this temperature for a certain time. The liquid products of different periods were obtained via a sampling valve and the gas product was collected by a sampling bag as reaction ended and cooled down to room temperature.

The liquid product were identified by GC–MS and quantified by a gas chromatography (Agilent 6890) with a FID detector and a capillary column (INNOWax, 30 m × 0.32 mm × 0.25 μm) with using cumene as the internal standard. The gas products were qualified by a GC 9800 chromatography equipped with a FID and a packed column (Porapak-Q column, 3 m × 3 mm) for C_1–C_4 alkanes and another GC 9800 equipped with a TCD and a packed column (TDX-01 column, 3 m × 3 mm) for CO, CO_2 and CH_4.

Conversion of methyl heptanoate (X_A) and selectivity of product i (S_i) are defined as:

$$X_A = \frac{C_0 - C_t}{C_0} \times 100\%$$

$$S_i(\mathrm{C-mol.\%}) = \frac{n_i * a_i}{(C_0 - C_t) * 8} \times 100\%$$

Here, C_0 refers to the initial concentration of methyl heptanoate and C_t means the concentration of final methyl heptanoate after

reaction; n_i indicates the moles of product i, and a_i represents the carbon numbers of product i.

3. Results and discussion

3.1. Catalyst properties

Fig. 1 shows the XRD patterns of Co/MgO, Co/SiO_2 and Co/Hβ catalysts with different Co loadings. MgO presented the typical face-centered cubic crystallography as evidenced by the significant diffractions at $2\theta = 36.9^\circ$, 42.8°, 62.3°, 74.8° and 78.7°, which are assigned to its (1 1 1), (2 0 0), (2 2 0), (3 1 1) and (2 2 2) planes, respectively [33]. As Co was supported on MgO, no diffractions corresponding to Co_3O_4 crystalline phase were observed even at low calcined temperature of 623 K and high Co loading of 10% (Fig. 1A), indicating that highly dispersed Co species was obtained on the surface of MgO. This was the same as the samples prepared by sequentially impregnating 5% and 10% of Co on the 10%Co/MgO-1273 K sample (Fig. 1C), which is well consistent with the previously reports [34–36]. As Co supported on MgO and calcined at elevated temperatures, complex structures containing Co_3O_4, MgO-CoO solid solution and $MgCo_2O_4$ spinel could form, which results in high dispersion of Co species on MgO with tiny sizes of Co_3O_4 below the XRD detection threshold [34]. In our cases, the formation of MgO-CoO solid solution was demonstrated by the magnified XRD patterns based on the (2 0 0) plane of MgO substrate (Fig. 1B). The calcined temperature of 823 K induced a shift of plane (2 0 0) of MgO to higher angle and the deviation increased with increasing the Co loadings, thanks to the discrepancy of Co^{2+} and Mg^{2+} radii resulted in contraction of unit cell of MgO-CoO solid solution. As the calcined temperature increased to 1273 K, besides the solid solution, another diffraction at $2\theta = 43.1^\circ$ was observed on 10%Co/MgO-1723 K, 5%Co-10%Co/MgO-1273 K-823 K and 10%Co-10%Co/MgO-1273 K-823 K (Fig. 1D), implying the existence of intermetallic $MgCo_2O_4$ spinel. At this calcined temperature, the diffractions of catalysts significantly intensified as compared with the pristine MgO, indicating the particles of catalyst agglomerated into larger sizes.

As Co supported on SiO_2 and Hβ with different Co loadings, the XRD patterns showed the different style when compared to the Co/MgO samples (Fig. 1E and F). Over 2.5%Co/SiO_2 and Co/Hβ with Co loadings of no more than 5%, no diffractions assigned to Co_3O_4 were observed, indicating high dispersion of Co species on these two supports. As Co loading was increased to 5% and above, the Co/SiO_2 catalysts presented diffractions corresponding to the cubic Co_3O_4 phase at $2\theta = 31.2^\circ$, 36.8°, 44.8°, 59.5° and 65.3° and their intensities increased with raising Co loadings, demonstrating that Co species aggregated into crystallites. Comparatively, the dispersions of Co_3O_4 in Co/Hβ were higher than those of Co/SiO_2, which is possibly due to the large surface of Hβ and the contained Al^{3+} with strong interaction with Co species.

Table 1 shows the textural properties and H_2-chemisorption results of the supported Co catalysts. Comparing to pristine MgO, the surfaces of Co/MgO catalysts significantly reduced while with the incremental mesoporous volumes and sizes as the calcined temperatures were no more than 823 K, which is attributed to that sintering of catalysts created more mesoporous spaces by particle stacking. The high calcined temperature of 1273 K resulted in a severe agglomeration, bringing about the surface and mesoporous volume of the catalyst remarkably decreased to less than 5 m^2/g and 0.01 cm^3/g, respectively, although its mesopore sizes were enlarged to 21 nm. After sequential Co impregnations on 10%Co/MgO-1273 K and calcined at 823 K, the surfaces, mesoporous volumes and sizes of catalysts significantly increased, which is created by the second supported Co species. As Co supported on SiO_2 and Hβ, the total surfaces and external surfaces (for Co/Hβ catalysts) and mesoporous volumes of catalysts dropped together with the slightly decreased and increased mesoporous sizes for Co/SiO_2 and Co/Hβ, respectively. Hβ zeolite is microporous and its surface is mainly contributed by its micropores. The surface of Co/Hβ showed a more significant decrease than Co/SiO_2, indicating that partial microchannels of Hβ are blocked by the supported Co species.

The dispersion and evaluated particles size of supported Co catalysts were analyzed by H_2-chemisorption technique (Table 1). With increasing Co loadings, their dispersions reduced with obtaining the incremental particle sizes. Although no diffractions of Co_3O_4 were observed on MgO even at the sequential 10% Co impregnation, the reduced Co/MgO catalysts showed the obvious Co particle sizes dependent on the calcined temperatures and Co loadings. This indicates that Co^{2+}/Co^{3+} cations could be reduced from the Co/MgO catalysts to form Co crystallites under our reduction procedure. Comparing to Co/MgO by once impregnation, the catalysts by the second impregnation showed larger Co particle sizes, which is due to that their relatively abundant Co cations in surface and/or subsurface could be easily reduced by H_2. No H_2 chemisorption took place for 10%Co/MgO-1273 K at our operation conditions, indicating that Co cation species in solid solution/spinel structures formed at this temperature is hardly reduced to the metallic state [37]. The BET and H_2-chemisorption results are well consistent with the XRD analyses.

Fig. 2 shows the H_2-TPR profiles of supported Co catalysts. The Co/MgO, Co/SiO_2 and Co/Hβ catalysts revealed several H_2 consumption peaks located in the wide range in terms of the calcined temperature and Co loadings. For Co/MgO catalysts (Fig. 2A), the peaks at low temperatures before 700 K corresponded to reduction of dispersed Co_3O_4 and the ones at medium of 700–1050 K and high (after 1050 K) temperatures were relative to the reduction of $MgCo_2O_4$ spinel and MgO-CoO solid solution, respectively, as indicated by the previous report [34]. The strong interactions between Co cations and Mg^{2+} via oxygen bridges in the solid solution and spinel lead to the reduction of suck kind Co species reduced at higher temperatures. As the catalysts calcined at higher temperatures or prepared with low Co loadings, the H_2 consumption of low temperatures shifted right while with those at higher temperatures almost unchanged, indicating that more Co^{2+} diffused into MgO matrix to form solid solution, and/or was oxided into Co^{3+} followed by reacting with MgO to form spinel. As the sequential Co impregnations on 10%Co/MgO-1273 K, however, the H_2 consumptions at high temperatures were remarkably reduced and the peaks at the medium temperatures were significantly enhanced (Fig. 2B), demonstrating that more spinel was formed during calcination procedure and reduced to obtain more metallic Co. For Co/SiO_2 catalysts with Co loadings of less than 5% (Fig. 2C), the H_2 consumptions at temperature of 550–750 K were assigned to sequential reduction of Co^{3+} to Co^{2+} followed by further reducing to Co^0 in Co_3O_4 [38]. At the Co loading of 10%, the two peaks relative to reduction of Co_3O_4 merged into the big one. Additionally, a distinct peak located at about 950 K was observed in Co/SiO_2 regardless of the Co loadings, implying the existence of cobalt oxide stabilized by support, such as cobalt silicate [39]. As Co supported on Hβ (Fig. 2D), the similar phenomena were observed with a little difference that the H_2 consumptions relative to Co_3O_4 reduction became wide and shifted to 500–850 K. The peaks at about 1050 K indicated the reduction of Co cations of strong interaction with Hβ.

Fig. 3 shows the CO_2-TPD patterns of Co/MgO (Fig. 3A) and NH_3-TPD profiles of Co/SiO_2 and Co/Hβ (Fig. 3B and C). A wide and superposed CO_2 desorption of pristine MgO indicated the existence of weak and medium basic sites, which is consistent with the previous report [40]. As Co was supported and calcined at elevated temperatures, the total basic sites significantly reduced. It seems that the basic sites with weak basicity dropped more

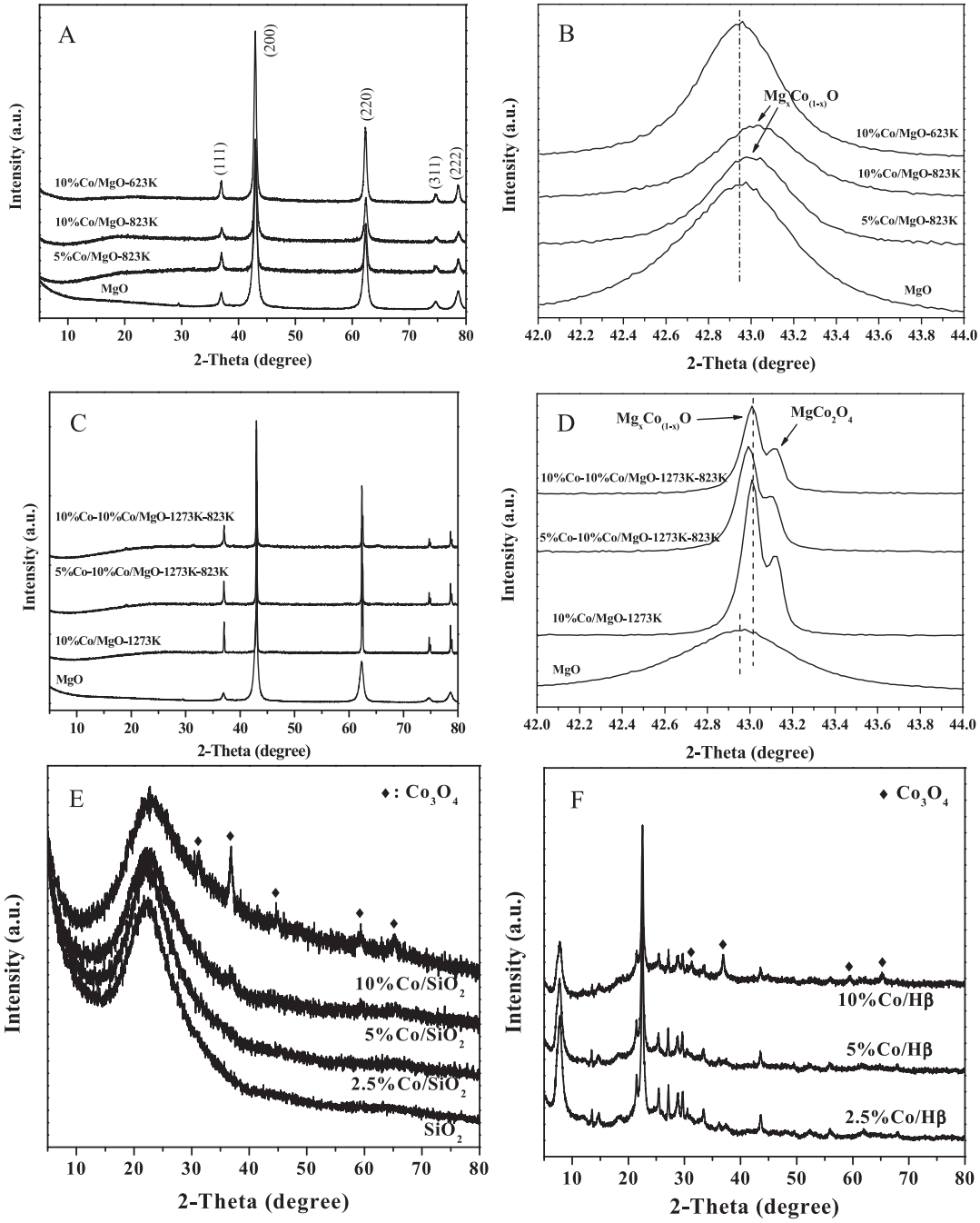

Fig. 1. XRD patterns of supported Co catalysts with different Co loadings: (A–D) Co/MgO, (E) Co/SiO_2 and (F) Co/Hβ.

fastly than the medium ones. With the second 10% of Co impregnated on 10%Co/MgO-1273 K and calcined at 823 K, very limited increment of basic sites was observed, indicating the basic sites of Co/MgO catalysts are mainly originated from MgO. The mediation of basic properties in Co/MgO are mainly affected by calcination temperature and impregnation mode, and the formation of solid solution and spinel structures significantly decreases the basic sites of Co/MgO catalysts. As Co supported on SiO_2, the NH_3-TPD profiles showed the sole NH_3 desorption peak of weak acidity at about 475 K and their acidic sites increased with increasing the Co loadings. As pure SiO_2 is inert, the creation of acidic sites by Co impregnation is perhaps ascribed to Co—O—Si domains in supported CoO_x and/or cobalt silicate [41]. Comparatively, Hβ showed weak and medium acidic sites at 500 K and 630 K, respectively. As Co supported on Hβ, apart from the weak and medium acidic sites, additional peaks of higher than 700 K indicated the existence of strong acidic sites. The weak and strong acidic sites increased with the position of strong ones shifting to lower temperatures as Co loadings increased. The strong acidity created by supported Co might be originated from the covalent connection of $Co^{\delta+}$ to framework Al^{3+} in micropores or external surface of Hβ [42].

3.2. Catalytic performance

Hydrogenolysis of methyl heptanoate to 1-heptanol/hydrocarbons was compared by Co/MgO, Co/SiO_2 and Co/Hβ, and the results were listed in Table 2. The detected products contained gaseous CO and C_1–C_3 alkanes (mainly contained CH_4,

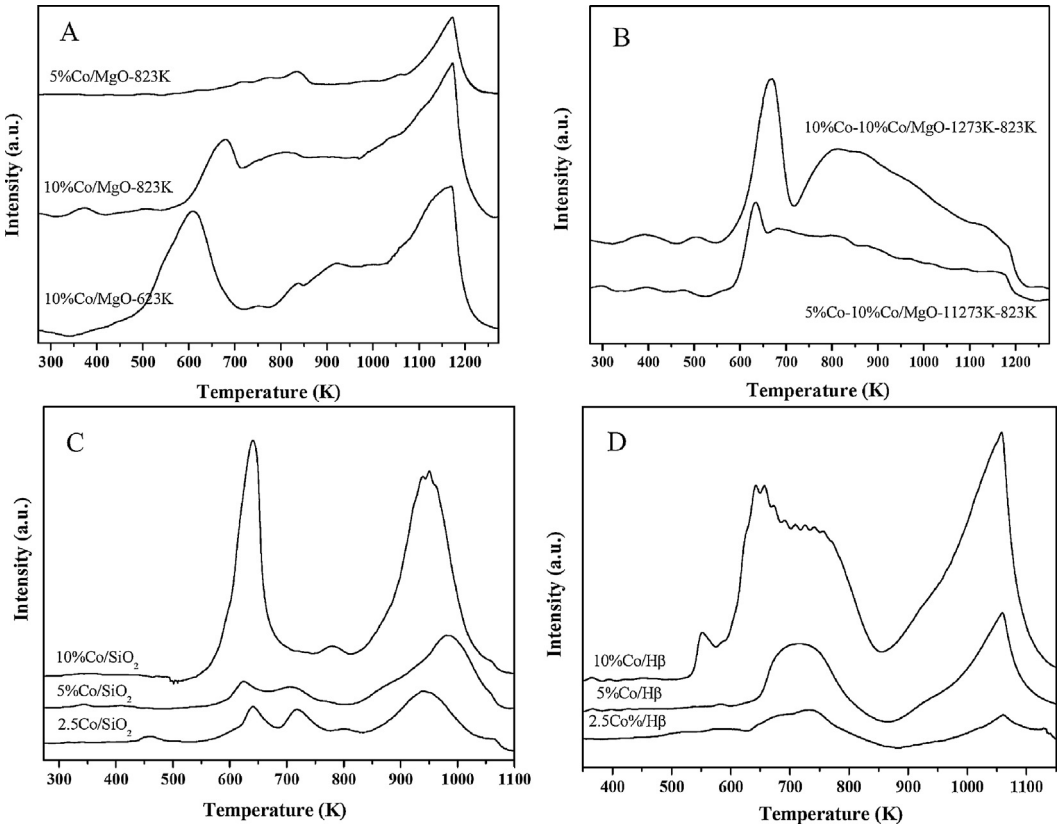

Fig. 2. H_2-TPR profiles of supported Co catalysts: (A–B) Co/MgO, (C) Co/SiO_2 and (D) Co/Hβ.

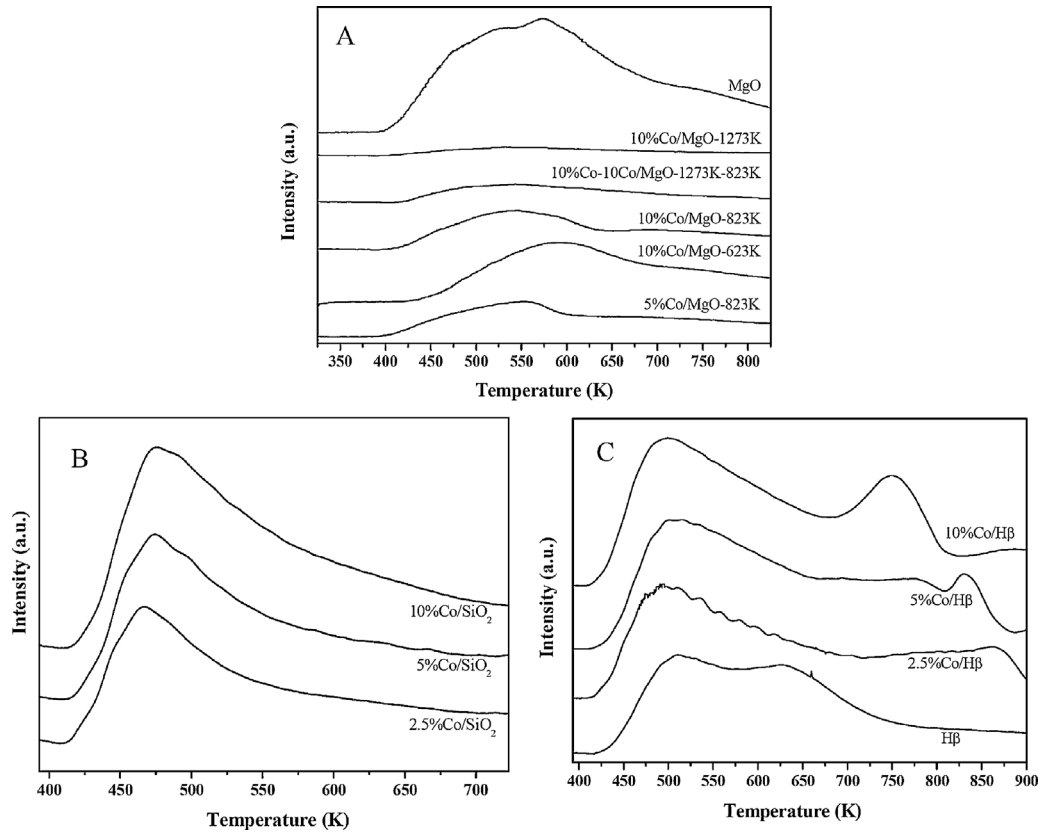

Fig. 3. CO_2-TPD curves of Co/MgO catalysts (A) and NH_3-TPD profiles of Co/SiO_2 (B) and Co/Hβ catalysts.

Table 1
The textural properties and H_2-chemisorption analyses of supported Co catalysts.

Catalyst	S_{BET}[a] (m^2/g)	S_{ex}[b] (m^2/g)	V_P[c] (cm^3/g)	Mesopore size[d] (nm)	Dispersion[e] (%)	Diamete[f] (nm)
MgO	126.0	–	0.37	2.0	–	–
5%Co/MgO-823 K	50.6	–	0.43	15.4	25.3	6.0
10%Co/MgO-623 K	92.5	–	0.65	8.3	10.8	15.7
10%Co/MgO-823 K	49.4	–	0.52	14.9	20.6	7.5
10%Co/MgO-1273 K	4.5	–	0.01	21.0	–	–
5%Co-10%Co/MgO-1273 K-823 K	12.1	–	0.09	8.0	13.1	10.4
10%Co-10%Co/MgO-1273 K-823 K	15.4	–	0.11	8.1	8.4	17.9
SiO_2	95.7	–	0.58	45.0	–	–
2.5%Co/SiO_2	95.8	–	0.52	41.0	25.8	5.2
5%Co/SiO_2	91.7	–	0.55	32.0	15.1	8.9
10%Co/SiO_2	80.3	–	0.50	37.2	6.4	19.3
Hβ	608.9	90.6	0.33	3.5	–	–
2.5%Co/Hβ	483.9	97.9	0.16	4.1	30.2	4.0
5%Co/Hβ	433.8	73.2	0.12	3.7	21.6	7.1
10%Co/Hβ	384.1	60.5	0.11	3.8	9.2	14.5

[a] Surface area calculated by BET method.
[b] External surface calculated by desorption branch by BJH method.
[c] Mesoporous volume calculated from desorption branch by BJH method.
[d] Mesopore size obtained by desorption branch by BJH method.
[e] Co particle dispersion.
[f] Diameter of Co particle.

not shown here), the liquid C_4 and C_5 (indicated as $<C_6$), C_6 and C_7 alkanes, oxygen contained methanol, heptanal, 1-heptanol, heptanoic acid and heptyl heptanoate. To ascertain stability of n-hexadecane solvent, the blank experiments were carried out at typical reaction condition by mixing n-hexadecane and freshly reduced catalysts. No conversion of n-hexadecane was observed over 10%Co/MgO-623 K and the very limited conversion of 3.2% was observed over 10%Co/Hβ, indicating that using n-hexadecane as solvent is feasible for hydrogenolysis of methyl heptanoate.

Co/MgO catalysts showed significant activities and high selectivities of more than 73% for 1-heptanol depending on calcination temperatures, Co loadings and impregnation modes. For the catalysts with low calcination temperature or high Co loading, the high methyl heptanoate conversions of more than 60% was obtained with major 1-heptanol, medium hexane, heptane and heptyl heptanoate and trace cracking $<C_6$ alkanes and methanol. As compared to Co/MgO prepared by once impregnation, the sequential impregnation on 10%Co/MgO-1273 K with the Co loadings of 5% and 10% significantly promoted conversion of methyl heptanoate and obtained the enhanced and reduced selectivities for hexane and heptyl heptanoate, respectively. Here, heptyl heptanoate is produced by transesterification of 1-heptanol and methyl heptanoate over the basic Co/MgO catalysts, and the transesterification activities improved over those with more basic sites and strong basicity, which is well consistent with the previous report [43]. More interestingly, the 10%Co/MgO-1273 K catalyst showed obviously reduced activity with 41.1% of heptanal, 14.2% of 1-heptanol and 42.2% of heptanoic acid and no other products were detected. For Co/SiO_2 and Co/Hβ, however, the conversions of methyl heptanoate distinctly increased with more than 75% of total C_6 and C_7 alkanes and little amounts of cracking alkanes, 1-heptanol and heptanoic acid. With increasing Co loadings, both of the Co/SiO_2 and Co/Hβ showed the enhanced activities as well as the selectivities of C_6 and cracking $<C_6$ alkanes, and the reduced heptanoic acid. Obviously, acid–base properties of support play the essential role in mediating their activities and product distributions. Distinct results observed over 10%Co/MgO-1273 K is possibly due to that acid originated from defects formed during reduction process [44] and base simultaneously present and induce hydrogenolysis of methyl heptanoate to heptanal and heptanoic acid via two different cracking pathways. Further transformations of these intermediates are suppressed owing to lack of enough metallic Co on this catalyst.

Fig. 4 shows the influence of hydrogenolysis of methyl heptanoate on reaction time over 10%Co-10%Co/MgO-1273 K-823 K and 10%Co/Hβ, respectively. With increasing reaction time, the conversion of the former catalyst raised significantly together with the slightly reduced 1-heptanol and increased C_6/C_7 alkanes and heptyl heptanoate (Fig. 4A). By comparison, the latter catalyst showed the significantly enhanced activities and almost complete conversion of methyl heptanoate was obtained at the period of 6 h

Table 2
Hydrogenolysis of methyl heptanoate over supported Co catalysts [a]

Catalyst	Conversion (%)	Product distribution (C-mol%)							
		$<C_6$	C_6	C_7	Methanol	Heptanal	1-Heptanol	Heptanoic acid	Heptyl heptanoate
10%Co/MgO-623 K	70.0	0.1	8.3	1.2	–	–	73.9	–	14.5
10%Co/MgO-823 K	64.9	0.1	9.1	1.3	0.2	0.2	75.1	–	10.8
10%Co/MgO-1273 K	13.6	–	–	–	–	41.1	14.2	42.2	–
5%Co/MgO-823 K	42.6	–	4.9	0.5	0.5	0.5	77.8	–	14.7
5%Co-10%Co/MgO-1273 K-823 K	59.1	0.2	14.6	1.7	–	0.2	77.0	–	3.9
10%Co-10%Co/MgO-1273 K-823 K	73.3	0.2	14.8	2.3	–	–	75.3	–	5.9
2.5%Co/SiO_2	71.5	2.0	35.4	40.2	–	–	0.4	9.7	–
5%Co/SiO_2	85.4	4.6	34.3	44.0	–	–	0.5	4.3	–
10%Co/SiO_2	98.3	8.1	45.1	45.6	–	–	0.2	0.3	–
2.5%Co/Hβ	86.0	3.5	33.8	45.1	–	–	0.5	4.6	–
5%Co/Hβ	89.7	7.6	39.3	44.0	–	–	0.4	1.8	–
10%Co/Hβ	99.7	13.7	43.3	38.5	–	–	0.1	0.4	–

[a] Methyl heptanoate 0.5 g, hexadecane 20 g, catalyst 0.15 g, reaction temperature 493 K, initial H_2 pressure 3.0 MPa, reaction time 20 h for Co/MgO and 6 h for Co/SiO_2 and Co/Hβ.

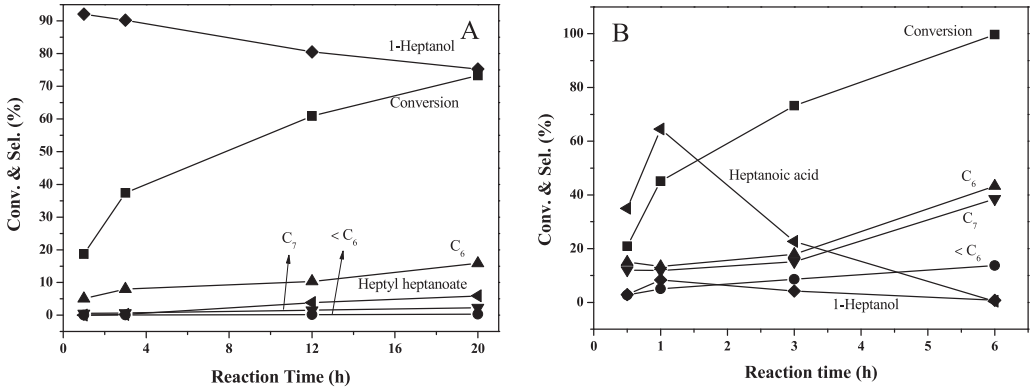

Fig. 4. Influence of reaction time on catalytic performance of supported Co catalysts in hydrogenolysis of methyl heptanoate: (A) 10%Co-10%Co/MgO-1273 K-823 K and (B) 10%Co/Hβ.

(Fig. 4B). By increasing reaction time, monotonous increment of cracking $<C_6$, C_6 and C_7 alkanes as well as the volcanoes of heptanoic acid and 1-heptanol were observed with the both maximal values at 1 h. These results indicate that 1-heptanol and heptanoic acid intermediates could be further converted into final hydrocarbons as hydrogenolysis proceeds.

Due to the acidic Co/Hβ catalysts presented heptanoic acid as the main intermediate in hydrogenolysis of methyl heptanoate, we further carried out hydrogenolysis of heptanoic acid under the same reaction condition to Fig. 4B and the results were listed in Fig. 5. The conversions of heptanoic acid increased with increasing reaction time and gained 73% of conversion at the ended 6 h. Meanwhile, significantly increased C_6 and C_7 alkanes and slightly raised cracking $<C_6$ alkanes were observed with reduced 1-heptanol and volcano heptyl heptanoate. These results reveal that 1-heptanol is produced at initial stage and combine with heptanoic acid to form heptyl heptanoate intermediate via esterification over this acidic catalyst. Comparing to hydrogenolysis of methyl heptanoate (Fig. 4B), the higher activation energy of heptanoic acid and heavy heptyl heptanoate intermediate results in the significantly lower conversion of heptanoic acid at the same ended time [45,46].

3.3. Hydrogenolysis pathway

During hydrogenolysis of fatty esters, three possible cracking pathways inducing the C—C bond adjacent to carbonyl group of ester, the acyl C—O and ether C—O bonds may take place and obtain the primary intermediates containing the hydrocarbons with chain lengths of one carbon less than the original fatty acids and methyl formate, the fatty aldehydes and methanol, and the fatty acids and methane, respectively [5,10]. Dissociative adsorption modes of fatty esters could be altered by changing geometries of metal active sites [18,47].

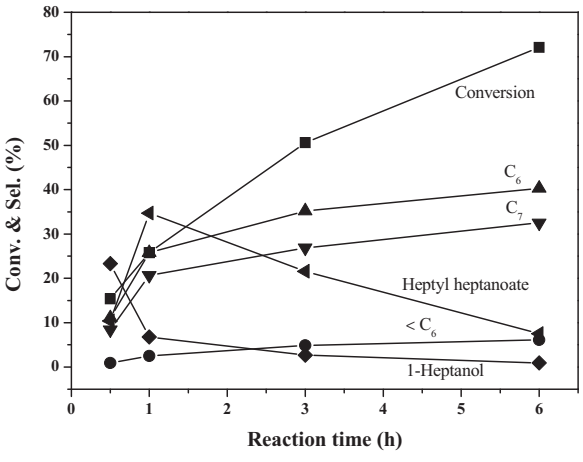

Fig. 5. Influence of reaction time on catalytic performance of 10%Co/Hβ catalyst in hydrogenolysis of heptanoic acid.

In our cases, this mediating effect is distinctly observed in hydrogenolysis of methyl heptanoate by altering support properties of Co catalysts. As Co supported on basic MgO, the main 1-heptanol with the selectivities of more than 73% and minor methanol and hetptanal in some cases was observed in Table 2, indicating that the basic sites of MgO promote formation of 1-heptanol. As shown in Scheme 1A, the acidic α-H of methyl heptanoate is captured by a basic site of MgO to form the carbanionic transition state accompanied with resonant oxygen anionic species, as it absorbs on Co/MgO. The $C^{\delta+}$ neighbored to oxygen atom in the oxygen anionic species is attracted by another basic site, which induces dissociation of acyl C—O bond to gain the absorbed methoxyl and hemiacetal moieties. These moieties are attacked by the spillover H atoms which are produced on adjacent Co to release methanol from methoxyl group and the absorbed hydride carbanionic species, the latter of which catches a H^+ from the former basic site to form heptanal. Most of heptanal could be further hydrogenated to 1-heptanol, which obtains the high selectivities of 1-heptanol via synergistic catalysis of metallic Co (H_2 activation) and basic MgO (dissociation absorption of methyl heptanoate). Here, higher alcohols could be otherwise produced by metal supported on base catalysts and the yields are higher than the previously reported Ru–SnO_x and Rh–SnO_x [8] and Co–SnO_x [17] catalysts. This base induced synergistic catalysis is very different from the previous reports that alcohols were produced via synergistic metal-acid catalysis [9,48]. Comparatively, as reaction proceeds, heptanoic acid intermediate is initially produced and consumed over acidic Co/Hβ catalysts (Fig. 4B). As shown in Scheme 1B, the acidic sites could catch the two oxygen atoms of methyl heptanoate and induce the ether C—O bond cracking to form the absorbed CH_3 species on Co and carbonium $C_6H_{13}COO$ with hyper conjugated structure. With attacking of spillover H atoms activated by neighbored Co, the CH_3 and $C_6H_{13}COO$ species are hydrogenated to CH_4 and hyper conjugated $C_6H_{13}COOH$ species, respectively, the latter of which releases from acidic site to form heptanoic acid for further transformation. Therefore, the Co/SiO_2 and Co/Hβ catalysts present the similarly synergistic H_2 activation over Co and dissociation absorption of methyl heptanoate over acid while with different cracking mode. As more reduced Co in Co/MgO, Co/SiO_2 and Co/Hβ, higher conversions of methyl heptanoate and yields of 1-heptanol and summed C_6/C_7 are observed, indicating that balance between metal and base/acid functionalities is achieved and significantly enhances methyl heptanoate transformations.

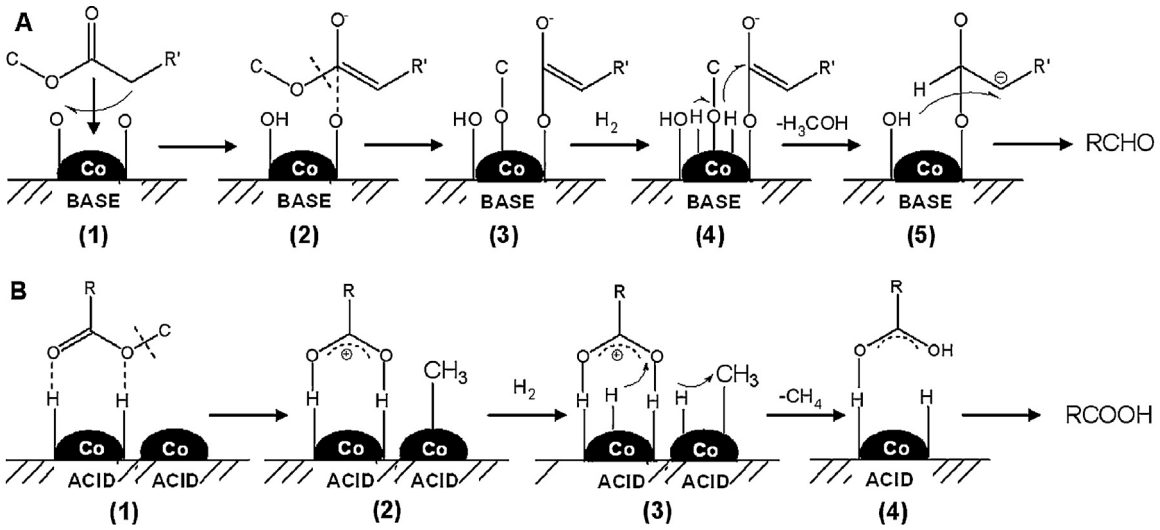

Scheme 1. Possible hydrogenolysis mechanism of methyl heptanoate over Co supported on base (A) and acid (B) catalysts.

Besides heptanal and heptanoic acid intermediates, minor C_6/C_7 alkanes over Co/MgO and the main counterparts with total amounts of more than 75% over Co/SiO_2 and $Co/H\beta$ are observed. Over Co/MgO catalysts, the formation of hexane and heptane is originated from decarbonylation of heptanal and HDO of 1-heptanol, respectively. The higher C_6/C_7 ratios obtained over Co/MgO than over Co/SiO_2 and $Co/H\beta$ indicate the facile decarbonylation of heptanal as compared to heptanoic acid. It seems that transformation of heptanal mainly proceeds via hydrogenation route to produce 1-heptanol and its parallel decarbonylation and/or consecutive HDO processes are significantly suppressed. Additionally, trace amounts of methanol, cracking $<C_6$ alkanes in liquid phase and significant CH_4 with minor CO in gas phase imply that methanol and CO could be fast hydrogenated to CH_4 and the cracking of C_6/C_7 alkanes has been suppressed. Over acidic Co/SiO_2 and $Co/H\beta$ catalysts, however, the comparable C_6 and C_7 are observed and the C_6/C_7 ratios increase with increasing Co loadings, which demonstrates that decarbonylation and HDO of heptanoic acid intermediate take place in parallel and the decarbonylation mainly occurs on metallic sites [49]. Acidic sites of catalysts promote dehydration of alcohol intermediate to alkene followed by further hydrogenation to C_7 alkane, which results in trace amounts of 1-heptanol in final liquid products [50]. Over Co/SiO_2 catalysts with weak acidity, the cracking products could be controlled within 8%, obtaining the maximal C_6/C_7 alkanes of more than 90% at 98% of methyl heptanoate conversion. The possible pathways in hydrogenolysis/HDO of methyl heptanoate are shown in Scheme 2, depending on the acid/base properties of catalysts.

Taking into account the similar molecular structure, we further use methyl acetate as the model compound of fatty esters for monitoring its hydrogenolysis process in real time. As shown in Fig. 6, Co/MgO presents CO, H_2O, CH_4, methanol and ethanol at the expense of methyl acetate, and no acetic acid is observed. This proposes that basic sites of Co/MgO indeed enhance the acyl C—O bond splitting of ester. Among these products, ethanol resultes from fast hydrogenation of primary acetaldehyde, and CH_4 and H_2O are originated from hydrogenation of methanol and CO, and/or decarbonylation of acetaldehyde. However, as methyl acetate absorbs on the acidic $Co/H\beta$ catalyst, its ether C—O bond is cracked into CH_4 and acetic acid at initial stage. Then the acetic acid intermediate is further decomposed to CO_2 and CH_4 by decarboxylation. H_2O is observed during this processing, which results from hydrogenation of CO_2 and/or acetic acid. No H_2O consumption in this hydrogenolysis demonstrates that the previously reported pathway of HDO of fatty esters is incorrect, where the production of heptanoic acid intermediate was proposed by hydrolysis of methyl heptanoate [50]. CO_2 other than CO is the exclusive deoxygenation product over $Co/H\beta$ in atmospheric pressure, which is different from our real HDO experiments. This discrepancy is attributed to that CO_2 is preferentially produced by decarboxylation under atmospheric and low pressures, while CO presents the main product by decarbonylation under high pressures, as indicated by the

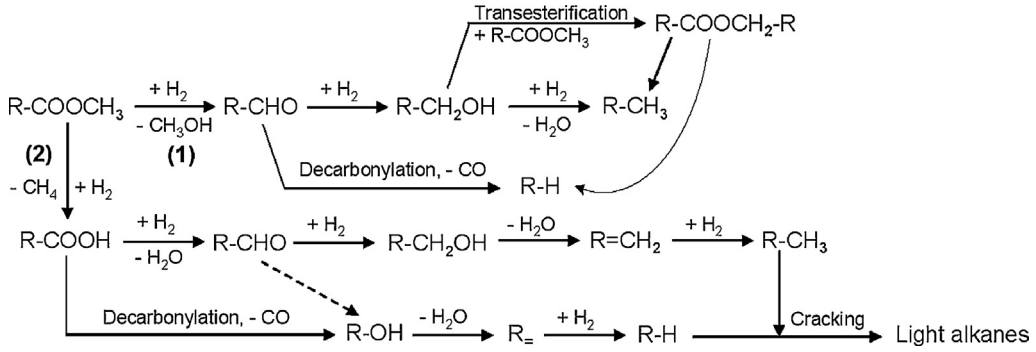

Scheme 2. Proposed reaction pathways over Co supported on base (pathway 1) and acid (pathway 2) catalysts in hydrogenolysis of methyl heptanoate.

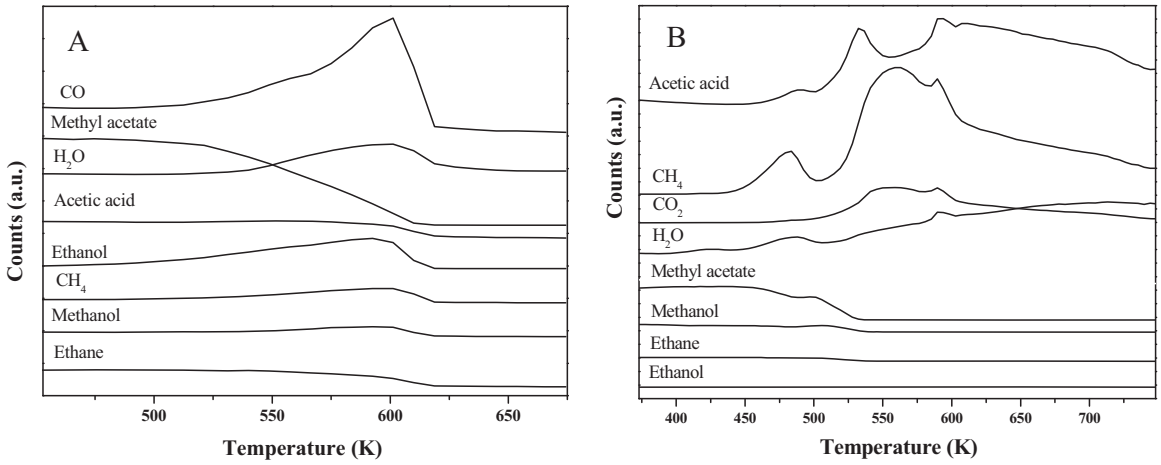

Fig. 6. TPSR experiments of supported Co catalysts in hydrogenolysis of methyl acetate: (A) 5%Co/MgO-823 K and (B) 5%Co/Hβ.

previous report [51]. It seems that the base mediated dissociation of ester is the rate-determined step because the ester disappeared synchronally with products and transformation of acid intermediate controls overall conversion of ester over the acidic catalysts. These TPSR experiments prove the proposed acid–base mediated dissociation routes in hydrogenolysis of fatty esters by us.

4. Conclusions

Co supported on basic MgO, neutral SiO_2 and acidic Hβ was prepared by incipient wetness impregnation. Co could highly disperse on MgO even at low calcined temperature and high Co loadings due to the formation of MgO-CoO solid solution and $MgCo_2O_4$ spinel. The sequential impregnation of Co on 10%Co/MgO-1273 K improved Co amounts on the surface/subsurface of catalysts, significantly reducing the dispersions with obtaining enlarged Co particle sizes by reduction. For Co/SiO_2 and Co/Hβ, the high Co dispersions at low Co loadings were possibly ascribed to the strong interactions between $Co^{\delta+}$ species and supports by covalent linkage via oxygen bridge. The formation of Co contained solid solution and spinel and $Co^{\delta+}$ species of strong interactions with supports resulted in their higher reduction temperatures and also significantly reduced basic sites depended on calcined temperatures and Co loadings over Co/MgO. As Co supported on SiO_2 and Hβ, the acidic sites of catalysts were increased with increasing the Co loadings. The weak acidity was created over Co/SiO_2 and weak, medium and strong acidities were observed over Co/Hβ. Hydrogenolysis of methyl heptanoate demonstrated that its acyl C—O bond initially splits into heptanal and methanol over basic Co/MgO, followed by further hydrogenation of heptanal to 1-heptanol, remaining more than 73% of 1-heptanol in final products. However, the ether C—O bond of methyl heptanoate is preferentially cracked to heptanoic acid and CH_4 over acidic Co/SiO_2 and Co/Hβ. The heptanoic acid intermediate is further transferred to more than 90% of summed C_6/C_7 alkanes by the parallel decarbonylation and HDO routes. This synergistic catalysis of metal and acid/base in our cases affords a methodology for facilely mediating product distribution in hydrogenolysis of vegetable oils.

Acknowledgements

The authors gratefully acknowledge the financial support from the National Basic Research Program of China (2012CB215304), the Natural Scientific Foundation of China (51161140331), the EU-China Cooperation for Liquid Fuels from Biomass Pyrolysis (246772) and the Natural Scientific Foundation of Guangdong Province (S2012040006992).

References

[1] M.H. Looi, S.T. Lee, S.B. Abd-hamid, Chinese Journal of Catalysis 29 (2008) 566–570.
[2] L. Rye, S. Blakey, C.W. Wilson, Energy & Environmental Science 3 (2010) 17–27.
[3] J.T. Kloprogge, L.V. Duong, R.L. Frost, Environmental Geology 47 (2005) 967–981.
[4] T.N. Kalnes, K.P. Koers, T. Marker, D.R. Shonnard, AICHE Journal 28 (2009) 111–120.
[5] T. Turek, D.L. Trimm, Catalysis Reviews: Science and Engineering 36 (1994) 645–683.
[6] D.S. Brands, G. U-A-Sai, E.K. Poels, A. Bliek, Journal of Catalysis 186 (1999) 169–180.
[7] S. Taniguchi, T. Makino, H. Watanuki, Y. Kojima, M. Sano, T. Miyake, Applied Catalysis A: General 397 (2011) 171–173.
[8] T. Miyake, T. Makino, S. Taniguchi, H. Watanuki, T. Niki, S. Shimizu, Y. Kojima, M. Sano, Applied Catalysis A: General 364 (2009) 108–112.
[9] Y. Pouilloux, F. Autin, C. Guimon, J. Barrault, Journal of Catalysis 176 (1998) 215–224.
[10] K.I. Gursahani1, R. Alcalá, R.D. Cortright, J.A. Dumesic, Applied Catalysis A: General 222 (2001) 369–392.
[11] H. Huang, S.H. Wang, S.J. Wang, G.P. Cao, Catalysis Letters 134 (2010) 351–357.
[12] H. Huang, G.P. Cao, C.L. Fan, S.H. Wang, S.J. Wang, Korean Journal of Chemical Engineering 26 (2009) 1574–1579.
[13] S.G. Liang, H.Z. Liu, J.L. Liu, W.T. Wang, T. Jiang, Z.F. Zhang, B.X. Han, Pure and Applied Chemistry 84 (2012) 779–788.
[14] B.X. Zhang, L. Lin, J.P. Zhuang, Y. Liu, L.C. Peng, L.F. Jiang, Molecules 15 (2010) 5139–5152.
[15] M.K. Gnanamani, G. Jacobs, R.A. Keogh, B.H. Davis, Journal of Catalysis 277 (2011) 27–35.
[16] Y. Pouilloux, F. Autin, A. Piccirilli, C. Guimon, J. Barrault, Applied Catalysis A: General 169 (1998) 65–75.
[17] K.D. Vigier, Y. Pouilloux, J. Barrault, Catalysis Today 195 (2012) 71–75.
[18] D.S. Brands, E.K. Poels, A. Bliek, Applied Catalysis A: General 184 (1999) 279–289.
[19] M. Mohammada, T.K. Hari, Z. Yaakob, Y.C. Sharma, K. Sopian, Renewable and Sustainable Energy Reviews 22 (2013) 121–132.
[20] O.V. Kikhtyanin, A.E. Rubanov, A.B. Ayupov, G.V. Echevsky, Fuel 89 (2010) 3085–3092.
[21] E. Lotero, Y. Liu, D.E. Lopez, K. Suwannakarn, D.A. Bruce, J.G. Goodwin, Industrial & Engineering Chemistry Research 44 (2005) 5353–5363.
[22] O.I. Senol, T.R. Vilyava, A.O.I. Krause, Catalysis Today 100 (2005) 331–335.
[23] R. Kumar, B.S. Rana, R. Tiwari, D. Verma, R. Kumar, R.K. Joshi, M.O. Garg, A.K. Sinha, Green Chemistry 12 (2010) 2232–2239.
[24] A. Guzman, J.E. Torres, L.P. Prada, M.L. Nuñez, Catalysis Today 156 (2010) 38–43.
[25] P. Mäki-Arvela, M. Snåre, K. Eränen, J. Myllyoja, D. Murzin, Fuel 87 (2008) 3543–3549.
[26] J. Hancsók, M. Krár, S. Magyar, L. Boda, A. Holló, D. Kalló, Microporous Mesoporous Materials 101 (2007) 148–152.
[27] N. Shi, Q.Y. Liu, T. Jiang, T.J. Wang, L.L. Ma, Q. Zhang, X.H. Zhang, Catalysis Communications 20 (2012) 80–84.
[28] H.L. Zuo, Q.Y. Liu, T.J. Wang, L.L. Ma, Q. Zhang, Q. Zhang, Energy & Fuels 26 (2012) 3747–3755.
[29] Y.X. Yang, C. Ochoa-Hernández, V.A. de la Peña O'Shea, J.M. Coronado, D.P. Serrano, ACS Catalysis 2 (2012) 592–598.

[30] J.X. Han, J.Z. Duan, P. Chen, H. Lou, X.M. Zheng, H.P. Hong, ChemSusChem 5 (2012) 727–733.
[31] S.F. Gong, A. Shinozaki, M.L. Shi, E.W. Qian, Energy & Fuels 26 (2012) 2394–2399.
[32] M. Snare, I. Kubickova, P. Maki-Arvela, K. Eranen, D.Y. Murzin, Industrial & Engineering Chemistry Research 45 (2006) 5708–5715.
[33] G. Dercz, K. Prusiki, L. Pajaki, R. Pielaszek, J.J. Malinowski, W. Pudlo, Materials Science-Poland 27 (2009) 201–207.
[34] H.Y. Wang, E. Ruckenstein, Applied Catalysis A: General 209 (2001) 207–215.
[35] T. Furusawa, A. Tsutsumi, Applied Catalysis A: General 278 (2005) 195–205.
[36] Y. Sharma, N. Sharma, G.V. Subba Rao, B.V.R. Chowdari, Solid State Ionics 179 (2008) 587–597.
[37] C.A. Querini, M.A. Ulla, F. Requejo, J. Soria, U.A. Sedrán, E.E. Miró, Applied Catalysis B: Environmental 15 (1998) 5–19.
[38] L. Shi, Y.Z. Jin, C. Xing, C.Y. Zeng, T. Kawabata, K. Imai, K. Matsuda, Y.H. Tan, N. Tsubaki, Applied Catalysis A: General 435/436 (2012) 217–224.
[39] S. Storsaeter, O. Borg, E.A. Blekkan, A. Holmen, Journal of Catalysis 231 (2005) 405–419.
[40] Z. Liu, W. Li, C.Y. Pan, P. Chen, H. Lou, X.M. Zheng, Catalysis Communications 15 (2011) 82–87.
[41] J.M. Rynkowski, T. Paryjczak, M. Lenik, Applied Catalysis A: General 106 (1993) 73–82.
[42] J.Q. Zhang, W.B. Fan, Y.Y. Liu, R.F. Li, Applied Catalysis B: Environmental 76 (2007) 174–184.
[43] F.R. Ma, M.A. Hanna, Bioresource Technology 70 (1999) 1–15.
[44] M.E. Miller, S.T. Misture, Journal of Physical Chemistry C 114 (2010) 13039–13046.
[45] S. Lestari, P. Mäki-Arvela, J. Beltramini, G.Q.M. Lu, D.Y. Murzin, ChemSusChem 2 (2009) 1109–1119.
[46] M.A. Natal Santiago, M.A. Sánchez-Castillo, R.D. Cortright, J.A. Dumesic, Journal of Catalysis 193 (2000) 16–28.
[47] L.J. Xu, Y. Xu, Catalysis Today 165 (2011) 96–105.
[48] O.A. Ferretti, J.P. Bournonville, G. Mabilon, G. Martino, J.P. Candy, J.M. Basset, Journal of Molecular Catalgsis 67 (1991) 283–294.
[49] E. Santillan-Jimenez, M. Crocker, Journal of Chemical Technology and Biotechnology 87 (2012) 1041–1050.
[50] O.I. Senol, E.M. Ryymin, T.R. Viljava, A.O.I. Krause, Journal of Molecular Catalysis A: Chemical 268 (2007) 1–8.
[51] J.G. Immer, H.H. Lamb, Energy & Fuels 24 (2010) 5291–5299.